

SC3D: Dynamic and Differentiable Causal Discovery for Temporal and Instantaneous Graphs

Sourajit Das¹ Dibyajyoti Chakraborty¹ Romit Maulik²

Abstract

Discovering causal structures from multivariate time series is a key problem because interactions span across multiple lags and possibly involve instantaneous dependencies. Additionally, the search space of the dynamic graphs is combinatorial in nature. In this study, we propose *Stable Causal Dynamic Differentiable Discovery (SC3D)*, a two-stage differentiable framework that jointly learns lag-specific adjacency matrices and, if present, an instantaneous directed acyclic graph (DAG). In Stage 1, SC3D performs edge preselection through node-wise prediction to obtain masks for lagged and instantaneous edges, whereas Stage 2 refines these masks by optimizing a likelihood with sparsity along with enforcing acyclicity on the instantaneous block. Numerical results across synthetic and benchmark dynamical systems demonstrate that SC3D achieves improved stability and more accurate recovery of both lagged and instantaneous causal structures compared to existing temporal baselines.

1. Introduction

The understanding of cause-effect relationships in a dynamical systems can be pivotal to make scientific discovery and reliable decisions. Many application fields such as climate and geophysical systems, neuroscience, biological systems and engineered networks, generate measurable data in the form of multivariate time series. In such situations, interactions can propagate over time as well instantaneously within a time slice. In general predictive models can be accurate without being causal whereas causal structure learning seeks to retrieve directed graphs which facilitates mechanistic intervention and under favorable assumptions, allows for reasoning under interventions and distribution shifts (Pearl,

¹College of Information Sciences and Technology, The Pennsylvania State University, University Park, USA ²School of Mechanical Engineering, Purdue University, West Lafayette, USA. Correspondence to: Sourajit Das <sjdas@psu.edu>.

Preprint. February 4, 2026.

2009; Peters et al., 2017). In this work, we propose the *Stable Causal Dynamic Differentiable Discovery (SC3D)*, a two-stage differentiable framework for causal discovery in multivariate dynamical systems that jointly learns both lag specific causal relationships and an instantaneous directed acyclic graph (DAG). Here *dynamic* refers to causal dependencies across time lags rather than time varying causal graphs.

One of the conventional approaches for causal discovery in time series data is based on the Granger style prediction (Granger, 1969) which measures directed dependencies by improving forecasting accuracy. This perspective inspired a large section of the research community to focus on lagged causal learning in nonlinear and vector autoregressive models. This includes constraint based methods and conditional independence testing curated for high dimensional data (Runge et al., 2019). Other methods leverage functional and distributional assumptions like non-Gaussianity, to detect directed structures in temporal networks such as VAR-LiNGAM (Hyvärinen et al., 2010). In the recent years, deep learning has also been exploited to parameterize nonlinear predictors and derive causal scores from learned temporal relationships (Tank et al., 2021; Nauta et al., 2019). In spite of the above progress, two challenges continue to be pressing for structural time series models: (i) jointly modeling lagged (inter) and instantaneous (intra) causalities, (ii) scaling the structure to larger number of variables without combinatorial search.

At the same time, differential causal discovery (DCD) has emerged as a powerful framework for learning directed acyclic graphs (DAGs) from observational data by formulating the structure learning as an optimization problem over a set of weighted adjacency matrices (Zheng et al., 2018). However, generic smooth acyclicity constraints can be numerically unstable and deteriorate very quickly beyond tens of variables (Nazaret et al., 2023). Stable Differentiable Causal Discovery (SDCD) addresses this challenge by (Nazaret et al., 2023), in which a numerically stable spectral acyclicity constraint and a two stage optimization technique, significantly improve scalability and robustness. For the case of time series, differentiable approaches like DYNOTEARs utilize the idea of continuous optimization

Table 1. Capabilities of representative baselines for temporal (lagged) and instantaneous causal discovery. “Instantaneous DAG” indicates an explicit acyclic intra-slice graph; “Nonlinear” indicates support for nonlinear dependencies.

Method	Lagged	Instantaneous	Nonlinear	Differentiable
SC3D	✓	✓	✓	✓
DYNOTEARs	✓	✗	✗	✓
PCMCI+	✓	✗	✓	✗
VAR-LiNGAM	✓	✓	✗	✗
NeuralGC (cMLP)	✓	✗	✓	✗
TCDF	✓	✗	✓	✗

for learning lagged structures (Pamfil et al., 2020). However, extension of robust and scalable methods in the differentiable domain to structural equation model (SEM) is still not fully explored.

In this paper, we propose a stable differentiable framework for causal discovery in multivariate dynamical systems with lagged and instantaneous effects. We study a structural vector autoregression (VAR) SEM where lagged edges represent the temporal propagation and the instantaneous edges represent intra-slice causal relationships. Motivated from the stability aspects of the SDCD model by (Nazaret et al., 2023), we present a two-step approach for dynamic causal discovery. Stage 1 conducts a node wise predictive screening over a time window to find candidate masks for lag-specific and instantaneous edges. Stage 2 refined these candidate masks through optimization of a likelihood based objective function, along with enforcing the spectral acyclicity penalty on the instantaneous block. This design ensures that the instantaneous block is acyclic while retaining the strengths of differentiable optimization while avoiding the problems of earlier smooth constraints (Zheng et al., 2018; Nazaret et al., 2023). We summarize our contributions to the paper below:

- We formulate causal discovery for dynamical systems using lag-specific adjacency matrices and instantaneous DAG components, bridging structural VAR models with stable differentiable causal discovery.
- We extend the two stage pruning and constraint approach of SDCD to the time series domain by screening candidate parents within a lagged predictor window prior to enforcing acyclicity constraint on the instantaneous matrix.
- We provide population level guarantees proving that Stage 1 preserves all true causal parents within the chosen temporal window, and that the acyclicity of the instantaneous dependencies implies acyclicity of the time unrolled graph.
- We evaluate SC3D on both synthetic and benchmark dynamical systems and demonstrate improved causal structure recovery over existing baselines.

2. Background and Related Work

The fundamental research on causal discovery from temporal data traces back to Granger causality, where causality is measured by improvement in forecasting by upon addition of past history of a variable to the model (Granger, 1969; Shojaie & Fox, 2022). This principle underlines a wide range of vector autoregressive (VAR) and nonlinear autoregressive models, which have been applied in econometrics, neuroscience, climate science and complex analysis (Kleinberg, 2013; Smith et al., 2011; Zhang et al., 2011). Conventional approaches consist of constraint based methods that leverage conditional independence testing such as PCMCI and PCMCI+ (Runge et al., 2019; Runge, 2020). These methods scale to moderately large systems although they rely heavily on test assumptions and hyperparameters. There is also the use of functional and distributional methods such VAR-LiNGAM, which exploit non-Gaussianity to recover directed temporal structures but require strict assumptions and deteriorate at higher dimensions (Hyvärinen et al., 2010).

In the recent years, researchers have explored neural parameterization of Granger causality using recurrent or convolutional neural network (RNN or CNN) architectures (Tank et al., 2021; Khanna & Tan, 2019; Marcinkevič & Vogt, 2021; Nauta et al., 2019). Despite such networks being capable of capturing nonlinear temporal relationships, these approaches predominantly focus on lagged interactions and do not model instantaneous causal relationships. Furthermore, RNNs are often sensitive to regularization and thresholding, rendering unstable causal discovery in sparse or high dimensional spaces. Amortized versions and representation learning approaches have relaxed some of the modeling assumptions but the result sacrifices structural guarantees (Löwe et al., 2022; Li et al., 2023).

Differential causal discovery has emerged to be a strong candidate for learning DAGs, by formulating the structure learning as a continuous optimization problem (Zheng et al., 2018). More recent advancements have attempted to further speed up the optimization efficiency theoretical properties using approaches such as topological swaps and alternative penalties and neural network parameterizations (Deng et al., 2023; Yu et al., 2019; 2021). However, most of these methods have utilized smooth trace-based acyclicity constraints, which can become numerically unstable or restrictive as the dimensions become large (Nazaret et al., 2023). So Stable Differentiable Causal Discovery (SDCD) solved this bottleneck by introducing a new kind of spectral acyclicity constraint along with a two-stage optimization strategy, significantly improving the scalability for static DAGs (Nazaret et al., 2023).

If we extend differential causal discovery to time series, we are faced with additional challenges, because such dy-

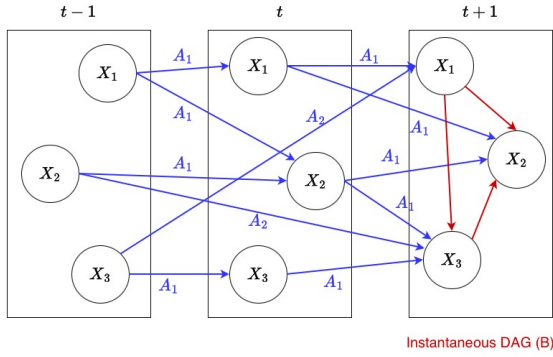


Figure 1. Structural vector autoregressive (SVAR) model with lagged and instantaneous causal dependencies. Nodes represent variables across time slices. Blue arrows denote lagged causal effects encoded by matrices $\{A_\ell\}_{\ell=1}^L$, while red arrows denote instantaneous causal relationships encoded by a directed acyclic graph B . SC3D jointly estimates both components, enforcing acyclicity only on the instantaneous block.

namic temporal systems display both lagged (inter-slice) and instantaneous (intra-slice) relationships. Although DYNOTEARs (Pamfil et al., 2020) adapts continuous time optimization to VAR models, it focuses mainly on the lagged structure does not effectively handle instantaneous effects. Relatedly, UnCLE (Bi et al., 2025) performs scalable causal discovery in nonlinear temporal systems with a focus on lagged dependencies, but does not model instantaneous causal graphs or enforce acyclicity constraints, making it complementary rather than directly comparable to the joint SVAR setting considered here. In general, existing methods either model lagged and instantaneous dependencies independently or suffer from scalability and stability issue when trying to learn both simultaneously. Unlike the existing methods, SC3D is motivated from the ideas of SDCD and temporal modeling into a unified framework for structural VAR systems. We combine node-wise temporal preselection with constrained optimization that uses a spectral and 2 cycle penalty applied only on the instantaneous causal structure to recover both lagged and instantaneous causal structure in a scalable and stable way. This approach which avoids numerical instabilities of smooth acyclicity and tackles joint dynamic causal discovery remains underexplored.

3. Methodology

Let us consider $\{X_t\}_{t \in \mathbb{Z}}$ to be a d -dimensional time series with $X_t = (X_t^1, \dots, X_t^d)$ generated by a *structural vector autoregressive* (SVAR) model or *structural equation model* (SEM). We assume the data is generated by the SVAR,

$$X_{t+1} = B^* X_{t+1} + \sum_{\ell=1}^L A_\ell^* X_{t+1-\ell} + \varepsilon_{t+1}, \quad (1)$$

where $A_\ell^* \in \mathbb{R}^{d \times d}$ denote lag- ℓ causal adjacency matrices, $B^* \in \mathbb{R}^{d \times d}$ represents instantaneous causal effects, and ε_{t+1} is i.i.d. noise independent of past variables. We assume $(I - B^*)$ is invertible and that the directed graph induced by B^* is acyclic. Once the data generated by the SVAR model in (1), the goal of causal discovery is to recover the lagged causal matrices $\{A_\ell\}_{\ell=1}^L$ and the instantaneous causality matrix B , corresponding to the ground-truth parameters $\{A_\ell^*\}_{\ell=1}^L$ and B^* . The lagged edges in A_ℓ denote the causal relationships moving forward in time, whereas the instantaneous edges in B represent the causal relationships among the variables within the same time slice, specifically we are interested with the current time slice $t + 1$. Figure 1 depicts the SVAR structure with lagged and instantaneous dependencies used in our study. Therefore, by construction, the lagged edges are ordered by time and cannot form any directed cycles. On the other hand, instantaneous edges are required to satisfy an acyclicity constraint to guarantee a well defined structural model.

This problem is challenging because we have to account for a combinatorial search space due to the joint lagged and instantaneous dependencies, as well as numerical instability when enforcing acyclicity constraints in high dimensional spaces. In order to address these challenges, we propose SC3D, a two-stage differentiable framework for causal discovery in multivariate dynamical systems comprising of both lagged and instantaneous dependencies. The proposed method takes a multivariate time series as input and gives the outputs: (i) lag-specific adjacency matrices encoding temporal inter-slice causal relationships and (ii) an instantaneous directed acyclic graph (DAG) representing intra-slice causal relationships. The overall design is motivated from the the stability and scalability aspects of differential causal discovery, while explicitly utilizing the temporal ordering intrinsic to time-series data.

In Stage 1, we perform temporal screening for each target variable (node) by fitting conditional predictive models using a fixed time window of candidate parents. This step identifies a sparse set of candidate lagged and instantaneous edges by removing weak dependencies while keeping all true causal parents at the population level. The output of Stage 1 is a pair of binary masks that limit the admissible lagged and instantaneous edges in the next stage. In Stage 2, we refine the causal structure by re-optimizing the model parameters under the masks from Stage 1 while enforcing acyclicity on the instantaneous adjacency matrix. We gradually increase the penalty coefficient until the instantaneous graph becomes acyclic, following which we keep it fixed. This design utilizes the time ordering of the lagged edges to ensure numerical stability and controlled optimization for the instantaneous structure.

3.1. Stage 1: Node-wise Temporal Preselection

Stage 1 aims to narrow down the search space by removing unlikely causal edges early while retraining all true dynamic parents with high probability. This is accomplished by node-wise temporal screening, which discovers possible lagged and instantaneous parents for all variables without any acyclicity constraint. For each target variable X_{t+1}^j , let us consider a temporal predictor window

$$\mathcal{V}_t^{(j)} := \{X_{t+1}^{-j}, X_t, X_{t-1}, \dots, X_{t+1-L}\}.$$

which includes the lagged variables up to order L and, if instantaneous effects are allowed, contemporaneous variables without self-loops. This window defines the pool of candidate parents for X_{t+1}^j .

Now we define the *dynamic Markov boundary* within the window $\mathcal{V}_t^{(j)}$, denoted by $MB^{\text{dyn}}(j)$ is the minimal set $S \subseteq \mathcal{V}_t^{(j)}$ such that

$$X_{t+1}^j \perp\!\!\!\perp \mathcal{V}_t^{(j)} \setminus S \mid S.$$

Intuitively, $MB^{\text{dyn}}(j)$ includes all lagged and contemporaneous variable within the window that directly affect the data generating process of X_{t+1}^j .

At the population level, this stage is equivalent to maximizing a penalized conditional log-likelihood over subsets of predictors. For any subset $S \subseteq \mathcal{V}_t^{(j)}$, we define the Stage-1 (population) score

$$\Psi_j(S) := \sup_{\theta: \text{supp}(\theta) \subseteq S} \mathbb{E}[\log p_\theta(X_{t+1}^j \mid X_S)] - \lambda|S|. \quad (2)$$

where p_θ represents a conditional predictive model parameterized by θ and $\lambda > 0$ controls the sparsity. Theorem 3.1 highlights the role of Stage 1 and proves that the pre-selection step does not discard any true dynamic parents within the temporal window.

Theorem 3.1. *Using the assumptions enlisted in Appendix A.1, there exists $\lambda_0 > 0$ such that for all $0 < \lambda \leq \lambda_0$, any maximizer*

$$S_j^* \in \arg \max_{S \subseteq \mathcal{V}_t^{(j)}} \Psi_j(S) \quad (3)$$

contains the dynamic Markov boundary for X_{t+1}^j . In particular,

$$MB^{\text{dyn}}(j) \subseteq S_j^*, \quad (4)$$

i.e. Stage 1 does not discard any true dynamic parents in the window.

Here, $\Psi_j(S)$ denotes the Stage-1 population objective for node j , defined as the penalized conditional log-likelihood over predictors S . The assumptions of Theorem 3.1 and its

proof are derived in Appendix A.2. The proof is inspired by population-level selection arguments used in SDCD for static DAGs (Nazaret et al., 2023), and is adapted to fit the temporal SVAR setting in our case.

In reality, we fit node-wise conditional models that predict X_{t+1}^j from subsets of $\mathcal{V}_t^{(j)}$, parameterized using differentiable predictors. The edge weights are then extracted from the grouped input layer weight magnitudes, producing non-negative scores for each lagged and instantaneous parent. The sparsity is enforced through ℓ_1 regularization on these group magnitudes. The learned group magnitudes are thresholded to create binary masks for lagged and instantaneous edges which are then used in Stage 2.

Stage-1 Optimization In practice, Stage 1 can be implemented by optimizing the empirical version of the population score in (2). Specifically, for each node j , we aim to solve

$$\hat{\theta}_j = \arg \max_{\theta} \frac{1}{n} \sum_{t=1}^n \log p_\theta(X_{t+1}^j \mid X_{\mathcal{V}_t^{(j)}}) - \lambda \|\theta\|_1, \quad (5)$$

where the ℓ_1 penalty enhances sparsity in the learned input groups. The resulting group magnitudes are then thresholded to generate the binary masks to be used in Stage 2.

3.2. Stage 2: Constrained Structure Refinement with Spectral Acyclicity

Stage 2 learns the causal structure by refining the model parameters based on the mask which were obtained in Stage 1, but this time with the intention of enforcing acyclicity on the instantaneous causal graph. All the disallowed edges from Stage 1 are now set to zero and the optimization is limited to the remaining lagged and instantaneous candidates. We now optimize regularized likelihood objective function that encourages sparsity in both the lagged and instantaneous adjacency matrices. This constrained re-optimization significantly reduces the search space and stabilizes training in high-dimensional settings.

Let $\{A_\ell\}_{\ell=1}^L$ denote the set of lag-specific adjacency matrices and B denote the instantaneous adjacency matrix. Since lagged edges move forward in time by design, they do not need additional constraints. Thus, we enforce an explicit constraint only on the instantaneous block B .

Stage-2 Optimization Problem Using the binary masks we obtained in Stage 1, we restrict both the lagged and instantaneous edges to the corresponding masked entries. Let $\{A_\ell\}_{\ell=1}^L$ be the set of lagged adjacency matrices and B denote the instantaneous adjacency matrix. The goal is to estimate these matrices by minimizing a regularized negative log-likelihood function, while enforcing acyclicity on the instantaneous block B . Concretely, the Stage-2

optimization problem can be written as follows:

$$\begin{aligned} \min_{\{A_\ell\}_{\ell=1}^L, B} \quad & \mathcal{L}_{\text{LL}}(\{A_\ell\}, B) - \alpha \sum_{\ell=1}^L \|A_\ell\|_1 \\ & - \beta \|B\|_1 - \lambda_{2c} \|B \odot B^\top\|_1 \\ \text{s.t.} \quad & \rho(B) = 0, \end{aligned} \quad (6)$$

where \mathcal{L}_{LL} is the log-likelihood of the node-wise conditional models, $\|\cdot\|_1$ is the ℓ_1 norm which promotes sparsity, and $\rho(B)$ denotes the spectral radius of B .

This approach provides a numerically stable alternative to smooth trace based acyclicity constraints (Nazaret et al., 2023). The spectral radius tends to enforce global acyclicity but it does not explicitly prevent short directed cycle during the optimization. When dealing with instantaneous graphs of large dimensions, it is possible to encounter strong 2-cycles composed of pairs of opposing edges that may satisfy a small spectral radius but potentially lead to unstable or ambiguous causal assignments. In order to address, we augment the spectral constraint with a 2-cycle penalty $\|B \odot B^\top\|_1$, which directly penalizes the reciprocal instantaneous edges. This additional term reinforces identifiability and stabilizes optimization in high dimensional regimes without negating the smoothness and scalability properties.

In order to prevent the over penalization of the acyclicity constraint, we adopt a gradual penalty schedule. In other words, we begin with gamma set to zero and increase gamma linearly during the training phase. At regular intervals, we extract a DAG from the current estimate of B by retaining the highest magnitude edges that preserve acyclicity. Once the extracted instantaneous graph satisfies the acyclicity constraint in terms of the target edge budget, we fix the penalty coefficient γ for the rest of the training. This approach impedes the oscillatory behavior and stabilizes optimization upon convergence.

Since the lagged edges are only able to connect nodes from successive time steps, it is sufficient to impose acyclicity on the instantaneous block B to guarantee that the acyclicity of the time-unrolled causal graph. The following proposition formalizes this insight showing that enforcing acyclicity on the instantaneous block alone is sufficient to guarantee acyclicity of the time-unrolled graph.

Proposition 3.2. *Let us consider a time window $T \in \mathbb{N}$, time unrolled graph generated by the dynamic SEM (1) over the window $\{X_1, \dots, X_T\}$ with instantaneous edges denoted as B^* and lag- ℓ edges denoted as A_ℓ^* . If the directed graph generated by B^* is acyclic, then the time unrolled graph over the window $\{1, \dots, T\}$ is acyclic for any $\{A_\ell^*\}_{\ell=1}^L$.*

The proof of Proposition 3.2 is given in Appendix A.3.

3.3. Algorithm

The first stage of SC3D performs node-wise temporal pre-selection in order to determine potential lagged and instantaneous edges. In Stage 2, it refines the causal structure via optimization of regularized likelihood objective function based on the resulting masks while ensuring acyclicity on the instantaneous block through a spectral acyclicity. The algorithm 1 in Appendix B outlines the proposed two-stage approach for the dynamic causal discovery along with the important hyperparameters considered in the experiments.

3.4. Computational complexity.

Let $n = N(T - L - 1)$ denote the number of training pairs after forming the temporal design window. Using the node-wise predictors of hidden width H , Stage-1 screening requires $\mathcal{O}(E_1 n d H (dL + d_{\text{inst}}))$ time, where $d_{\text{inst}} = d$ when instantaneous condition is used and 0 otherwise. Stage-2 operates on masked inputs and costs $\mathcal{O}(E_2 n d H (\rho_{\text{lag}} dL + \rho_{\text{inst}} d))$ plus a spectral acyclicity overhead of $\mathcal{O}(E_2 (n/B) K d^2)$ from K step power iterations. Complete details are provided in Appendix C.

4. Numerical Results

4.1. Scalability with respect to Dimension

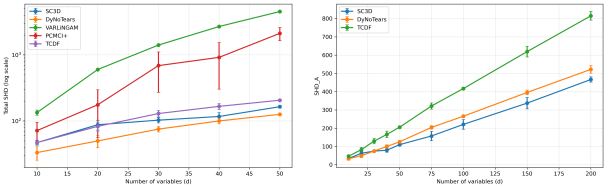


Figure 2. Scalability of causal structure recovery under increasing dimension ($L = 3, T = 200$). **Left:** Total structural Hamming distance $\text{SHD}_{\text{total}}$, accounting for both lagged and instantaneous errors, shown on a logarithmic scale. **Right:** Lagged-only structural error SHD_A shown on a linear scale for methods which model lagged dependencies, enabling a direct comparison for temporal structure recovery.

We analyze how causal structure recovery methods scale with number of variables under the nonlinear SVAR model in (1). Specifically, we set the lag order to $L = 3$ and time horizon $T = 200$, vary the dimension given from the set $d \in \{10, 20, 30, 40, 50\}$, while keeping the expected graph sparsity constant. Additionally, we average the results across five seeds to compare the performance across different baselines. Figure 2 (left) presents our plots the total structural Hamming distance, $\text{SHD}_{\text{total}} = \sum_{\ell=1}^L \text{SHD}(A_\ell) + \text{SHD}(B)$, on logarithmic scale to accommodate the large dynamic range across methods and dimensions. Here, we set $B \equiv 0$ and count all true instantaneous edges as skipped for methods that do not model instanta-

neous causality (eg., DYNOTEARs, PCMCI+). Given this unified evaluation, SC3D has the lowest or comparable total SHD performance across all dimensions, whereas PCMCI+ and VAR-LiNGAM exhibit rapid increase in SHD performance as the dimension d increases.

To separate the scalability with regards to temporal lag only structure, Figure 2 (right) illustrates the lag-only error SHD_A for SC3D and DYNOTEARs in a linear scale to earmark absolute differences in lag recovery. Even though SC3D, DYNOTEARs and TCDF outperform the classical baselines in terms of scalability, it is clearly evident that SC3D consistently achieves lower SHD_A even when dimensions increase which showcases more accuracy in recovery of lagged dependencies. Moreover, the low variance across random seeds indicate stable optimization and structural recovery. In summary, we can say that SC3D demonstrated robust lagged structure learning along with stable handling of instantaneous effects, which accounts for its exceptional scalability to high dimensional regimes.

4.2. Decomposing Lagged and Instantaneous Structure Recovery

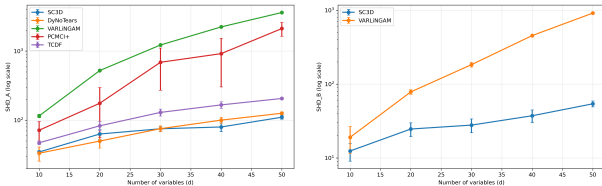


Figure 3. Decomposition of structural error into lagged and instantaneous components for the d -sweep experiment ($L = 3$, $T = 200$). Left: lagged structure error. Right: instantaneous structure error.

Figure 3 breaks down the total structural error shown in Figure 2 into contributions from lagged and instantaneous components to identify the areas of the improvements. For each method, the lagged error reflects mismatches in the estimated temporal adjacency matrices across all lags. The instantaneous error captures mistakes in the recovered intra-slice causal graph. As observed in the left panel, SC3D consistently achieved lower lagged error SHD_A than PCMCI+ and VAR-LiNGAM across all dimensions. SC3D stays competitive with DYNOTEARs and TCDF but exceeds the performance after $d = 40$. Importantly, the lagged error of SC3D increases slowly as d grows and shows low variability, which suggests stable recovery of temporal dependencies in higher dimensional regimes.

On the other hand, the instantaneous error breakdown in the right panel reveals a more notable advantage. Among the methods that explicitly model instantaneous effects, SC3D significantly outperforms VAR-LiNGAM, with about an order of magnitude reduction in SHD_B as the dimension

increases. This gap widens for larger d , highlighting the benefits of enforcing a stable acyclicity constraint while employing two-stage screening while learning instant DAGs. Methods that do not estimate instant structure (like DYNOTEARs, PCMCI+, TCDF) effectively equate to $B \equiv 0$ in this setting, incurring unavoidable instantaneous errors. Together, these results indicate that the improved scalability of SC3D stems from gains in both lagged and instant structure recovery.

4.3. Ranking performance via AUROC and AUPRC

Next, we assess the ranking quality of the estimated causal relationships using certain threshold free evaluation metrics: area under the receiver operating characteristics curve (AUROC) and area under the precision-recall curve (AUPRC). These evaluation metrics are particularly meaningful if the underlying causal graph is sparse. For lagged causal relationships, we compute the aggregated scores obtained by considering the maximum absolute edge scores across all lags for every ordered variable pair and comparing it to the ground truth presence of any lagged edge. The instantaneous AUROC and AUPRC is reported only if the methods explicitly estimates an instantaneous adjacency matrix. Table Table 2 summarizes our results on a typical dimension $d = 30$; other dimensions' results, although not illustrated, behave similarly.

As can be seen in Table 2, SC3D is found to generate strong lagged ranking performance, with AUROC and AUPRC comparable to or exceeding existing temporal baselines such as DYNOTEARs and PCMCI+. At the same time, it significantly outperforms the lagged models TCDF and Neural Granger Causality (CMLP), which exhibit near-random ranking over lagged relationships. More importantly, SC3D is the only method that is found to simultaneously achieve good ranking accuracy for instantaneous causal relationships. Methods that do not estimate instantaneous effects (eg., DYNOTEARs, PCMCI+, TCDF and cMLP) cannot rank such relationships and therefore posses unavoidable bottlenecks in the SVAR settings. Overall, the above results show that SC3D addresses a strictly harder causal discover problem by jointly ranking lagged and instantaneous dependencies while maintaining competitive performance.

4.4. Sensitivity to Lag Order

We now analyze how the proposed SC3D framework behaves as we increase the maximum lag order L in the framework. This analysis is not intended to compare scalability in terms of dimensions to other baselines models since most competing methods either do not explicitly model large lag orders or tend to be computationally infeasible beyond a small value of L . Instead, we aim to evaluate the robustness of SC3D to increasing temporal depths. We fix the number

Table 2. Aggregated lagged and instantaneous AUROC/AUPRC at $d = 30$ ($L = 3$, $T = 200$). Reported values are mean \pm standard deviation over five random seeds. Methods that do not model instantaneous effects are marked as “ \times ” for the corresponding metrics.

METHOD	AUROC _A \uparrow	AUPRC _A \uparrow	AUROC _B \uparrow	AUPRC _B \uparrow
SC3D	0.910 \pm 0.009	0.766 \pm 0.028	0.811 \pm 0.036	0.715 \pm 0.061
DYNOTEARNS	0.858 \pm 0.022	0.722 \pm 0.044	\times	\times
PCMCI+	0.890 \pm 0.022	0.778 \pm 0.029	\times	\times
TCDF	0.503 \pm 0.006	0.050 \pm 0.010	\times	\times
cMLP	0.500 \pm 0.000	0.047 \pm 0.006	\times	\times

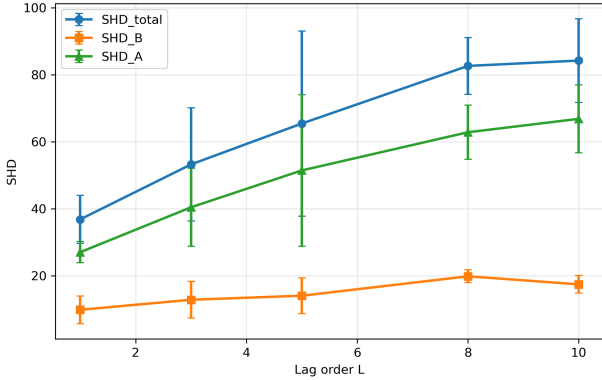


Figure 4. Sensitivity of SC3D to lag order L ($d = 8$, $T = 200$). The total structural error increases gradually as L grows, while the instantaneous component remains well controlled, indicating stable optimization and robustness to increasing temporal depths.

of variables to $d = 8$ and time horizon $T = 200$, and sweep over the lag order $L \in \{1, 3, 5, 8, 10\}$. We aggregated the results over five random seeds for each L . We plot the total SHD, along with the decomposition into lagged and instantaneous components.

Figure 4 shows that the total SHD increases gradually with an increase in L , reflecting the complexity of the underlying graph. The plot demonstrates smooth growth without any fluctuations, ensuring that our two stage screening process has controls the search space even as additional lagged dependencies are introduced. The instantaneous component remains under control for all values of L , indicating that the effectiveness of enforcing acyclicity only on the instantaneous block. In general, the test demonstrates the scalability of SC3D with respect to the moderately large depth levels without numerical instability or significant deterioration in structure recovery.

4.5. Performance across dynamical systems

We evaluate the performance of the SC3D on different benchmark and synthetic dynamical systems intended to investigate various aspects of temporal causal discovery such as chaotic dynamics, nonstationarity and nonlinear long-range dependencies. Details of these datasets and governing equations are mentioned in Appendix D.

4.5.1. LORENZ96 - CHAOTIC DYNAMICS.

The performance is next evaluated in Lorenz96 system, a commonly used chaotic benchmark with sparse local interactions. Here, the causal relationships are purely lagged with no instantaneous effects and the ground truth reveals fixed indegree pattern. Thus, we study the lagged recovery in terms of top- k approach with $k = 3$ incoming edges per target, along with aggregated AUROC and AUPRC capturing threshold independent ranking performance.

Table 3 presents the results at a representative dimension $d = 20$. SC3D attains the lowest top- k structural error among all baselines while exhibiting significantly lower variances across seeds. Moreover, it attains the highest AUROC and AUPRC, showcasing accurate and stable ranking of the true causal parents in this chaotic regime. In contrast, DYNOTEARNS and cMLP (Neural Granger) behave similarly to random rankings and show much higher structural error, while PCMCI+ shows high error and variability. Overall these results prove SC3D remains robust under challenging lag-only dynamics while also maintaining scalability and stability.

4.5.2. TIME-VARYING STRUCTURAL EQUATION MODEL (TVSEM).

Next, we evaluate the performance of SC3D on a time-varying structural equation model (TVSEM) where the direction of causality reverses over time. This system oscillates between two regimes in non-overlapping time intervals where the dominant lagged dependency switches between $X_{t-1} \rightarrow Y_t$ and $Y_{t-1} \rightarrow X_t$. This example dataset explicitly tests the ability of our method to track a changing direction of causality over time rather than just averaging them out. Figure 5 depicts the scores for the Lag-1 edge for all windows considered in the task. In the left panel, we show the results for SC3D while the right panels puts together the baselines (DYNOTEARNS and PCMCI+). The shaded regions in the plots denote the first regime and the unshaded regions denote switched or second regime.

SC3D showcases a distinct and consistent separation of the two directional scores, with the dominant edge smoothly adapting to the change of regime. On the contrary, baseline methods display higher score magnitudes but exhibit

Table 3. Lorenz96 (chaotic dynamics): lagged structure recovery at $d = 20$ with lag order $L = 1$ and horizon $T = 200$ (top- k evaluation with $k = 3$). Reported values are mean \pm standard deviation over five random seeds. Since Lorenz96 contains no instantaneous effects, all metrics are reported for the lagged component only.

METHOD	$\text{SHD}_A (\text{TOP-}k) \downarrow$	$\text{AUROC}_A (\text{AGG}) \uparrow$	$\text{AUPRC}_A (\text{AGG}) \uparrow$
SC3D	35.6 ± 1.5	0.833 ± 0.000	0.719 ± 0.000
PCMCI+	66.4 ± 12.1	0.739 ± 0.055	0.438 ± 0.088
DYNOTEARNS	102.0 ± 0.0	0.500 ± 0.000	0.158 ± 0.000
NEURALGC (cMLP)	102.0 ± 0.0	0.500 ± 0.000	0.157 ± 0.000

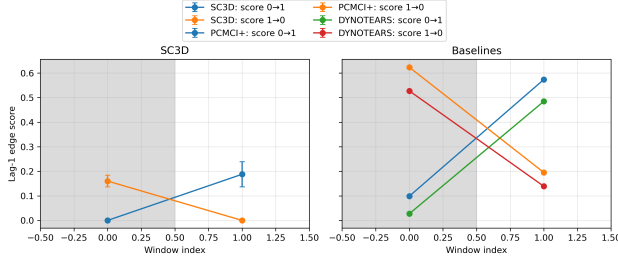


Figure 5. TVSEM regime switching direction tracking using windowed evaluation (lag order $L = 1$). Left: SC3D. Right: baselines (DYNOTEARNS and PCMCI+). SC3D displays smoother and temporally consistent score trajectories that fit well to regime changes while baselines show sharper but less stable transitions throughout windows.

less consistent behavior across the regimes, which indicates reduced sensitivity to temporal changes in directionality. Although all the methods attain perfect window-level directional accuracy in this low-dimensional setup, the score trajectories reveal significant differences. SC3D has more stable and interpretable directional information over time whereas the baselines tend to depend on sharper but more rigid score transitions. The above results reflect the advantage of SC3D in tracking evolving causal relationships in nonstationary dynamical systems.

4.5.3. NONLINEAR CONTINUOUS 8-VARIABLE (NC8) SYSTEM.

Table 4. Nonlinear Continuous 8-variable dataset (NC8): aggregated ranking performance for lagged causal structure ($d = 8$, $L = 4$, $T = 200$). NC8 contains no instantaneous effects, so all metrics correspond to lagged structure only.

Method	$\text{AUROC}_A^{\text{agg}} \uparrow$	$\text{AUPRC}_A^{\text{agg}} \uparrow$
SC3D	0.885 ± 0.004	0.828 ± 0.007
PCMCI+	0.900 ± 0.008	0.804 ± 0.025
DYNOTEARNS	0.653 ± 0.021	0.410 ± 0.007
NeuralGC (cMLP)	0.500 ± 0.000	0.161 ± 0.000

Finally, we consider lagged causal discovery for a low dimensional nonlinear dynamical system ($d = 8$) which has structured long-range temporal edges without any instantaneous edges. The graph in this setting only has lagged edges, so in addition to SHD_A , we use the threshold-free methods for ranking that are averaged over time lags.

As seen in Table 4, the PCMCI+ has the best AUROC score,

reflecting excellent performance in global ranking performance on this small-scale system. However, SC3D has the best AUPRC score, which is typically informative on sparse causal graphs, where precision at high confidence is crucial. The performance of DYNOTEARNS and NeuralGC is significantly lower which can be attributed to their aggressive sparsification strategies and sensitivity to thresholding. In summary, these findings indicate that while PCMCI+ has excellent performance in overall ranking, SC3D has significantly better accuracy in identifying true causal parents among the top ranked edges. This underscores SC3D’s ability to find stable and highly precise nonlinear lagged dependencies rather than optimizing performance for a single threshold.

4.6. Ablation Study

We perform an ablation study to analyze the how the key components of SC3D operate on lower ($d = 20$) and large ($d = 40$) dimensions. As shown in Table 5, we can observe that disabling Stage 1 preselection results in a drastic increase in the SHD values and a collapse in the instantaneous F1 score, demonstrating its importance in controlling the search space. Further disabling penalty freezing or the 2-cycle penalty degrades the instantaneous recovery, especially at high dimensions. We provide full quantitative results in the Appendix D.4.1.

5. Conclusion

We present SC3D, a stable, scalable and differentiable framework for causal discovery in multivariate dynamical systems with both lagged and instantaneous relationships. By combining node-wise temporal preselection along with constrained optimization subject to a spectral acyclicity penalty, SC3D facilitates scalable structure learning while avoiding numerical instabilities of smooth acyclicity constraints. Our proposed method, demonstrated strong and stable performance across a range of synthetic, nonlinear and chaotic benchmarks. It tackles a more challenging causal discovery problem than existing temporal methods. Future work will focus on extensions to nonstationary and online settings that exhibit delays and instantaneous effects simultaneously.

Impact Statement

This paper presents a methodological work which aims to advance causal discovery in multivariate dynamical systems. The proposed framework is tested exclusively on synthetic and benchmark datasets. While causal discovery methods may eventually inform decision making in scientific and engineering applications, we do not foresee any immediate ethical or societal consequences which require specific discussion at this stage.

References

Bi, T., Pan, Y., Jiang, X., Sun, H., Ma, M., and Wang, P. Uncle: Towards scalable dynamic causal discovery in non-linear temporal systems. *arXiv preprint arXiv:2511.03168*, 2025.

Deng, C., Bello, K., Aragam, B., and Ravikumar, P. K. Optimizing NO-TEARS objectives via topological swaps. In *Proceedings of the 40th International Conference on Machine Learning*, pp. 7563–7595. PMLR, 2023.

Granger, C. W. J. Investigating causal relations by econometric models and cross-spectral methods. *Econometrica*, pp. 424–438, 1969.

Hyvärinen, A., Zhang, K., Shimizu, S., and Hoyer, P. O. Estimation of a structural vector autoregression model using non-gaussianity. *Journal of Machine Learning Research*, 11(5), 2010.

Khanna, S. and Tan, V. Y. F. Economy statistical recurrent units for inferring nonlinear granger causality. *arXiv preprint arXiv:1911.09879*, 2019.

Kleinberg, S. *Causality, probability, and time*. Cambridge University Press, 2013.

Li, H., Yu, S., and Principe, J. Causal recurrent variational autoencoder for medical time series generation. *arXiv preprint arXiv:2301.06574*, 2023.

Lorenz, E. N. Predictability: A problem partly solved. In *Proc. Seminar on Predictability*, volume 1, 1996.

Löwe, S., Madras, D., Zemel, R., and Welling, M. Amortized causal discovery: Learning to infer causal graphs from time-series data. In *Conference on Causal Learning and Reasoning*, pp. 509–525. PMLR, 2022.

Marcinkevičs, R. and Vogt, J. E. Interpretable models for granger causality using self-explaining neural networks. *arXiv preprint arXiv:2101.07600*, 2021.

Nauta, M., Bucur, D., and Seifert, C. Causal discovery with attention-based convolutional neural networks. *Machine Learning and Knowledge Extraction*, 1(1):19, 2019.

Nazaret, A., Hong, J., Azizi, E., and Blei, D. Stable differentiable causal discovery. *arXiv preprint arXiv:2311.10263*, 2023.

Pamfil, R., Sriwattanaworachai, N., Desai, S., Pilgerstorfer, P., Georgatzis, K., Beaumont, P., and Aragam, B. Dynotears: Structure learning from time-series data. In *International Conference on Artificial Intelligence and Statistics*, pp. 1595–1605. PMLR, 2020.

Pearl, J. *Causality*. Cambridge University Press, 2009.

Peters, J., Janzing, D., and Schölkopf, B. *Elements of Causal Inference: Foundations and Learning Algorithms*. MIT Press, 2017.

Runge, J. Discovering contemporaneous and lagged causal relations in autocorrelated nonlinear time series datasets. In *Conference on uncertainty in artificial intelligence*, pp. 1388–1397. Pmlr, 2020.

Runge, J., Nowack, P., Kretschmer, M., Flaxman, S., and Sejdinovic, D. Detecting and quantifying causal associations in large nonlinear time series datasets. *Science Advances*, 5(11):eaau4996, 2019.

Shojaie, A. and Fox, E. B. Granger causality: A review and recent advances. *Annual Review of Statistics and Its Application*, 9:289–319, 2022.

Smith, S. M., Miller, K. L., Salimi-Khorshidi, G., Webster, M., Beckmann, C. F., Nichols, T. E., Ramsey, J. D., and Woolrich, M. W. Network modelling methods for fmri. *NeuroImage*, 54(2):875–891, 2011.

Tank, A., Covert, I., Foti, N., Shojaie, A., and Fox, E. B. Neural granger causality. *IEEE Transactions on Pattern Analysis and Machine Intelligence*, 44(8):4267–4279, 2021.

Yu, Y., Chen, J., Gao, T., and Yu, M. DAG-GNN: DAG structure learning with graph neural networks. In *Proceedings of the 36th International Conference on Machine Learning*, 2019.

Yu, Y., Gao, T., Yin, N., and Ji, Q. DAGs with no curl: An efficient DAG structure learning approach. In *Proceedings of the 38th International Conference on Machine Learning*, pp. 12156–12166. PMLR, 2021.

Zhang, D. D., Lee, H. F., Wang, C., Li, B., Pei, Q., Zhang, J., and An, Y. The causality analysis of climate change and large-scale human crisis. *Proceedings of the National Academy of Sciences*, 2011.

Zheng, X., Aragam, B., Ravikumar, P. K., and Xing, E. P. Dags with no tears: Continuous optimization for structure learning. *Advances in neural information processing systems*, 31, 2018.

A. Theoretical Analysis

A.1. Assumptions for Stage 1

1. For each node j , the true conditional $p^*(X_{t+1}^j \mid \mathcal{V}_t^{(j)})$ belongs to the model class $\{p_\theta(\cdot \mid \cdot)\}_\theta$.
2. The joint distribution of $(X_{t+1}, X_t, \dots, X_{t+1-L})$ has a strictly positive density on its support.
3. If a variable $W \in \mathcal{V}_t^{(j)}$ appears with a nonzero structural coefficient in (1) for node j (either an instantaneous parent in B^* or a lagged parent in some A_ℓ^*), then X_{t+1}^j is not conditionally independent of W given $\mathcal{V}_t^{(j)} \setminus \{W\}$.

A.2. Proof of Theorem 3.1

Proof. Let us consider a node j and abbreviate $\mathcal{V} := \mathcal{V}_t^{(j)}$. For any subset $S \subseteq \mathcal{V}$, we can write the expected conditional log-likelihood as

$$\sup_{\theta: \text{supp}(\theta) \subseteq S} \mathbb{E}[\log p_\theta(X_{t+1}^j \mid X_S)] = C_j - \inf_{\theta: \text{supp}(\theta) \subseteq S} \mathbb{E}[\text{KL}(p^*(\cdot \mid \mathcal{V}) \parallel p_\theta(\cdot \mid X_S))] \quad (7)$$

where $C_j = \mathbb{E}[\log p^*(X_{t+1}^j \mid \mathcal{V})]$ does not depend on S . Thus, maximizing (2) is equivalent (up to the constant C_j) to minimizing

$$\mathcal{L}_j(S) := \underbrace{\inf_{\theta: \text{supp}(\theta) \subseteq S} \mathbb{E}[\text{KL}(p^*(\cdot \mid \mathcal{V}) \parallel p_\theta(\cdot \mid X_S))] + \lambda|S|}_{\eta_j(S) \geq 0} \quad (8)$$

Let $B := MB^{\text{dyn}}(j)$. By definition, conditioning on B is sufficient, thus the model is well-specified on B and we have $\eta_j(B) = 0$. For any strict superset $S \supsetneq B$, we can ignore extra variables in parameters, so $\eta_j(S) = 0$ as well. But we have $|S| > |B|$, and therefore $\mathcal{L}_j(S) > \mathcal{L}_j(B)$.

Now consider any subset S that does not contain B . By assumption of strict faithfulness and strict positivity, omitting any element of B induces a strictly positive KL gap: $\eta_j(S) > 0$ whenever $B \not\subseteq S$. Therefore, there exists λ_0 such that for all $0 < \lambda \leq \lambda_0$, we have $\eta_j(S)$ dominating the sparsity advantage $\lambda(|B| - |S|)$ for any S with $B \not\subseteq S$.

Therefore B (or an equivalent minimal boundary when non-unique) is the minimizer of $\mathcal{L}_j(\cdot)$, and any minimizer corresponds to a maximizer of $\Psi_j(\cdot)$. □

A.3. Proof of Proposition 3.2

We consider the time unrolled directed graph corresponding to (1). Next we consider a time window $T \in \mathbb{N}$ and define the vertex set

$$\mathcal{U}_{1:T} := \{(t, j) : t \in \{1, \dots, T\}, j \in [d]\}$$

We consider two types of directed edges: (i) lagged edges across time slices, and, (ii) instantaneous edges within each time slice:

$$\begin{aligned} (t - \ell, i) \rightarrow (t, j) &\iff (A_\ell^*)_{ji} \neq 0, \quad \ell \in \{1, \dots, L\}, \quad t - \ell \geq 1 \\ (t, i) \rightarrow (t, j) &\iff (B^*)_{ji} \neq 0, \quad i \neq j. \end{aligned}$$

We denote the resulting directed graph by $\mathcal{G}_{1:T}$.

Proof. We observe that the directed graph generated by B^* is acyclic in nature, thus it permits a topological ordering $\pi : [d] \rightarrow \{1, \dots, d\}$ such that for every instantaneous edge in $B_{ji}^* \neq 0$ i.e., $i \rightarrow j$, we have $\pi(i) < \pi(j)$.

Now lets define a strict lexicographic order \prec on vertices $(t, j) \in \mathcal{U}_{1:T}$:

$$(t_1, j_1) \prec (t_2, j_2) \iff \text{either } t_1 < t_2, \text{ or } (t_1 = t_2 \text{ and } \pi(j_1) < \pi(j_2)).$$

We observe that every directed edge in $\mathcal{G}_{1:T}$ points forward under the order \prec . In other words,

- *Lagged edges*: If $(t - \ell, i) \rightarrow (t, j)$ is a lagged edge, then $t - \ell < t$, thus $(t - \ell, i) \prec (t, j)$.
- *Instantaneous edges*: If $(t, i) \rightarrow (t, j)$ is an instantaneous edge, then we have $t = t$ and $\pi(i) < \pi(j)$ by definition, hence we have $(t, i) \prec (t, j)$.

Thus we observe that every edge points forward under the order \prec , and we can say $\mathcal{G}_{1:T}$ is acyclic in nature. \square

B. Algorithm and Hyperparameters

In all simulations, we use Adam optimization with different learning rate for both stages. Stage 1 is trained for $E_1 = 200$ epochs with sparsity coefficient $\lambda = 0.15$. In stage 2, we use learning rate $\eta_2 = 1.25 \times 10^{-3}$, $\alpha = 0.02$, $\beta = 0.001$, and $\lambda_{2c} = 0.05$, with a linear schedule for γ starting from zero. Penalty freezing is triggered when the extracted instantaneous DAG is acyclic and retains at least $\lfloor \eta(d)s_{\text{inst}}d \rfloor$ edges, where s_{inst} denotes the expected instantaneous indegree.

In all simulations, we set $s_{\text{inst}} = 2$. The retain fraction $\eta(d)$ is chosen adaptively based on dimension:

$$\eta(d) = \begin{cases} 0.5, & d \leq 6, \\ 0.65, & 7 \leq d \leq 20, \\ 0.8, & d > 20. \end{cases}$$

Algorithm 1 Dynamic Stable Differentiable Causal Discovery

Input: Multivariate time series $\{X_t\}_{t=1}^T$, lag order L , sparsity parameter λ

Output: Lagged adjacency matrices $\{A_\ell\}_{\ell=1}^L$, instantaneous DAG B

Stage 1: Node-wise temporal preselection

for $j = 1$ to d **do**

for epoch = 1 to E_1 **do**

 Update θ_j using Adam Optimizer

$$\mathcal{L}_j(\theta) = \arg \max_{\theta} \sum_t \log p_{\theta}(X_{t+1}^j \mid X_{\mathcal{V}_t^{(j)}}) - \lambda \|\theta\|_1$$

end for

 Compute edge scores as group norms of the first layer input weights

end for

Generate masks $\{\mathcal{M}_{A_\ell}\}, \mathcal{M}_B$ by thresholding

Stage 2: Constrained optimization for structure refinement

Initialize $(\{A_\ell\}, B)$ using Stage 1

$\gamma \leftarrow 0$

for epoch = 1 to E_2 **do**

 Update $(\{A_\ell\}, B)$ using Adam Optimizer

$$\mathcal{L} = \mathcal{L}_{\text{LL}} - \alpha \sum_{\ell} \|A_{\ell}\|_1 - \beta \|B\|_1 - \gamma \rho(B) + \lambda_{2c} \|B \odot B^T\|_1$$

Increase γ

if DAG extracted from B is acyclic and $|E(B)| \geq E_{\min}$ **then**

 Freeze γ

end if

end for

Return: $\{A_\ell\}_{\ell=1}^L, B$

C. Complexity Analysis

We evaluate the computational complexity of SC3D by segregating the costs of the Stage 1 (temporal preselection) and Stage 2 (constrained structure refinement). Let d be the number of variables, L be the maximum lag order, T be the time window, and N be the number of independent trajectories or samples. After constructing the temporal window, the total number of training samples is $n = N(T - L - 1)$.

Each node-wise predictor is parameterized by a neural network with a hidden layer of width H . Let E_1 and E_2 denote the number of optimization epochs used in Stage 1 and Stage 2. The mini-batch size is represented by B .

In Stage 1, SC3D, fits d independent node-wise predictive models. Each model takes the temporal predictor window as input

$$\mathcal{V}_t^{(j)} = \{X_{t+1}^{-j}, X_t, \dots, X_{t+1-L}\},$$

which has dimensionality $dL + d_{\text{inst}}$, where $d_{\text{inst}} = d$ if instantaneous mode is enabled and 0 otherwise. For each training step, the forward and backward passes scale linearly with the input dimension and hidden width. Therefore, the total time complexity of Stage 1 given to be

$$\mathcal{O}(E_1 n d H (dL + d_{\text{inst}})). \quad (9)$$

Stage 2 executes on the masked input space generated by Stage 1. Let $\rho_{\text{lag}} \in (0, 1]$ and $\rho_{\text{inst}} \in (0, 1]$ represent the fraction of retained lagged and instantaneous edges after preselection. The total input dimension per node reduces to $\rho_{\text{lag}} dL + \rho_{\text{inst}} d$. Thus the total optimization cost for Stage 2 is

$$\mathcal{O}(E_2 n d H (\rho_{\text{lag}} dL + \rho_{\text{inst}} d)). \quad (10)$$

Acyclicity overhead SC3D deploys a spectral radius penalty to enforce the acyclicity on the instantaneous adjacency matrix B via K steps of power iteration. This computation which is performed periodically typically costs $\mathcal{O}(Kd^2)$ per evaluation. If we consider all mini-batches and epochs, the total acyclicity overhead is

$$\mathcal{O}(E_2 (n/B) Kd^2). \quad (11)$$

Combining all components in (9), (10), and (11), the total runtime complexity of SC3D can be expressed as

$$\mathcal{O}(E_1 n d H (dL + d_{\text{inst}}) + E_2 n d H (\rho_{\text{lag}} dL + \rho_{\text{inst}} d) + E_2 (n/B) Kd^2). \quad (12)$$

D. Datasets

Inspired by the nonlinear temporal causal discovery scenarios studies in UnCLE (Bi et al., 2025), we modify the NC8 and TVSEM benchmarks to generate controlled ground truth dynamics and extract specific elements of lagged and time varying causal structure to suit our experiments.

D.1. Lorenz 96 Dataset

We generate time-series data using the Lorenz 96 dynamical system (Lorenz, 1996), a standard model for chaotic behavior. The system consists of d variables, x_1, \dots, x_d , governed by the differential equation:

$$\frac{dx_i}{dt} = (x_{i+1} - x_{i-2})x_{i-1} - x_i + F, \quad (13)$$

where indices are computed modulo d . The data is generated using an Euler discretization with additive Gaussian noise. The state update rule from time t to $t + 1$ is:

$$\mathbf{x}_{t+1} = \mathbf{x}_t + \Delta t \cdot \frac{d\mathbf{x}_t}{dt} + \sigma \cdot \boldsymbol{\epsilon}_t, \quad (14)$$

where $\boldsymbol{\epsilon}_t \sim \mathcal{N}(\mathbf{0}, \mathbf{I})$. The specific parameters used for the simulation are forcing constant $F = 8.0$, time step $\Delta t = 0.01$, noise scale $\sigma = 0.1$, and initialization: $\mathbf{x}_0 \sim \mathcal{N}(F \cdot \mathbf{1}, 0.01^2 \mathbf{I})$.

D.2. Time-Varying Structural Equation Model (TVSEM)

We simulate a non-stationary 2-dimensional system ($d = 2$) using a regime-switching Vector Autoregressive model. The state evolution follows the equation:

$$\mathbf{x}_t = \mathbf{A}^{(s_t)} \mathbf{x}_{t-1} + \boldsymbol{\epsilon}_t, \quad (15)$$

where $\boldsymbol{\epsilon}_t \sim \mathcal{N}(\mathbf{0}, \sigma^2 \mathbf{I})$ is Gaussian noise with scale $\sigma = 0.1$. The causal structure s_t alternates every 200 time steps. In the first regime, the coupling coefficients are set to 0.8 for $y \rightarrow x$ and 0.1 for $x \rightarrow y$. In the second regime, these coefficients shift to 0.2 and 0.7 respectively, effectively reversing the dominant causal direction while maintaining the same underlying graph skeleton.

D.3. NC8 Dataset

We utilize an 8-dimensional system ($d = 8$) with a lag order of $L = 4$ that integrates linear autoregressive decay with heterogeneous non-linear interactions. The state update rule is defined as:

$$\mathbf{x}_t = \text{clamp} \left(\sum_{\ell=1}^L \mathbf{A}^{(\ell)} \mathbf{x}_{t-\ell} + \boldsymbol{\Phi}(\mathbf{x}_{t-1}, t) + \boldsymbol{\epsilon}_t, -5, 5 \right) \quad (16)$$

where $\boldsymbol{\epsilon}_t \sim \mathcal{N}(\mathbf{0}, \sigma^2 \mathbf{I})$ and the linear weights $\mathbf{A}^{(\ell)}$ decay by a factor of $(\ell + 1)^{-1}$. The non-linear function $\boldsymbol{\Phi}$ applies distinct transformations to specific variables, including sinusoidal coupling, hyperbolic tangent activations, soft-cubic transformations $z \mapsto z^3(1 + |z|)^{-1}$, and ReLU-like interactions $\max(\cdot, 0)$, while variable x_4 acts as a time-dependent exogenous driver. The data is simulated with a noise scale of $\sigma = 0.1$ and bounded within $[-5, 5]$.

D.4. Additional Results

D.4.1. ABLATION EXPERIMENTS

Table 5. Ablation study for Dynamic-SC3D on VAR data.

Variant	$\text{SHD}_{\text{total}} \downarrow$	$\text{SHD}_B \downarrow$	$\text{F1}_B \uparrow$
<i>d</i> = 20			
Full (SC3D)	87.60 \pm 13.17	24.60 \pm 4.63	0.510 \pm 0.046
Linear predictor	79.00 \pm 10.97	25.20 \pm 5.23	0.586 \pm 0.069
No freezing	97.40 \pm 16.13	25.60 \pm 6.97	0.505 \pm 0.088
No 2-cycle penalty	94.20 \pm 12.70	25.60 \pm 3.77	0.487 \pm 0.037
No Stage 1	637.60 \pm 6.62	133.80 \pm 15.05	0.193 \pm 0.021
<i>d</i> = 40			
Full (SC3D)	116.80 \pm 15.04	37.20 \pm 6.52	0.730 \pm 0.075
Linear predictor	157.60 \pm 19.89	60.00 \pm 5.18	0.506 \pm 0.046
No freezing	148.80 \pm 42.13	46.00 \pm 12.05	0.618 \pm 0.130
No 2-cycle penalty	165.40 \pm 11.50	51.80 \pm 5.64	0.506 \pm 0.058
No Stage 1	2848.20 \pm 45.20	658.20 \pm 51.46	0.105 \pm 0.019